JOURNAL OF MATERIALS SCIENCE 18 (1983) 3105–3116

Macroscopic fracture surface energy of unidirectional metal matrix composites: experiment and theory

MINORU TAYA, AKIMASA DAIMARU
Department of Mechanical and Aerospace Engineering, University of Delaware, Newark, Delaware 19711, USA

A method of measuring the macroscopic frature surface energy γ_F is studied and its verification is made compared with the theoretical prediction. Metal matrix composites used in the experiment are unidirectional graphite fibre-reinforced 6061 aluminium. A good agreement between the experimental and theoretical results is obtained.

1. Introduction

As a structural material, composites of high performance in their mechanical properties, stiffness, strength and toughness are required. Though main emphasis has been placed on the enhancement of the stiffness and strength of composites, the requirement of higher toughness of composites is equally important for some cases of environments. Unfortunately these three properties are often conflicting to each other.

As to the measurement and prediction of the fracture toughness of unidirectional composites, a number of works have been made [1–6]. Application of linear elastic fracture mechanics (LEFM) [1] was led to the fact that the values of the critical stress intensity factor K_{Ic} did not reflect any basic materials property. Thus a number of researchers [2–6] developed models to account for the role of fibre in the initiation and propagation processes of the crack. However, none of the above works have focused on the correlation between the theoretical and experimental results except for a model study by Cooper [2] who used ductile fibres of rather large diameter.

In this paper the fracture surface energy (γ) of unidirectional metal matrix composites (MMC) is focused on. There are two ways of defining the fracture surface energy, the energy release rate for the initiation of the crack (γ_I) and the energy absorbed during the fracture averaged over the whole history of the fracture process (γ_F) [5]. For the purpose of evaluating the fracture toughness of metal matrix composites, the macroscopic surface energy (γ_F) is more suitable than γ_I. Then a question arises as to what experimental method is the best suited to measure γ_F and then how to verify the experimental results. In order to obtain γ_F, one must obtain first the total fracture energy (W_F) by an appropriate test. The most popular testing method to measure W_F is the three-point bending specimen with a notch at the midpoint. This method was first explored by Nakayama [7] for ceramic materials and modified later by Tattersall and Tappin [8] who used triangular notches at the midpoint. Both methods give us force–displacement (P–δ) curve which is integrated to yield W_F. By the above method, a crack propagation is well controlled, thereby it is suitable for brittle materials. Following the above pioneering works, a number of researchers have used the three-point bending test specimen with triangular notches [9, 10] or a side notch [11] at the midpoint.

We have recently made a preliminary study [12] on the prediction of γ_F to account for the elastic energy and plastic work during the propagation of a penny-shaped crack which existed initially inside a MMC specimen. This study has been further developed in this paper to estimate the macroscopic fracture surface energy γ_F which will be verified by a special three-point bending test.

0022–2461/83 $03.00 + .12

2. Theoretical model

Consider an unidirectional metal matrix composite specimen which contains a penny-shaped crack as an initial flaw. It is assumed in our model that the penny-shaped crack is located inside the MMC specimen and is perpendicular to the fibre axis. Under the applied stress (strain) along the fibre axis, the penny-shaped crack is assumed to grow in a concentric manner. The above three-dimensional crack propagation can be simulated by the two-dimensional model as shown in Fig. 1 if the concept of volume average is used [6]. In this two-dimensional model the cylindrical fibre is assumed to be of rectangular section.

There are three mechanisms contributing to the fracture energy W_F, elastic strain energy, plastic work along the matrix–fibre interface near the crack plane and fibre pull-out. It is noted here that unlike polymer based composites metal matrix composites usually have a strong interface bonding, hence pull-out should be very limited.

2.1. Elastic strain energy release rate ($\bar{G}$)

Here we assume the condition of iso-strain:

$$\epsilon_0 = \frac{\sigma_m}{E_m} = \frac{\sigma_f}{E_f} \tag{1}$$

where ϵ_0 is the strain applied along the fibre axis (the y-axis), σ_m and σ_f are the stresses in the matrix and fibre domain, respectively, and E_m and E_f are the Young's moduli of the matrix and fibre material, respectively. In order to estimate the elastic strain energy release rate of the composite ($\bar{G}$), the averaging process is employed (Fig. 2). Those variables averaged are denoted by the upper bar. Then under the iso-strain condition, the volume averaged Young's modulus, stress and energy release rate are given by, respectively,

$$\bar{E} = \frac{aE_m + dE_f}{a+d} = V_m E_m + V_f E_f \tag{2}$$

$$\bar{\sigma} = \frac{a\sigma_m + d\sigma_f}{a+d} = V_m \sigma_m + V_f \sigma_f \tag{3}$$

$$\bar{G} = \lim_{\Delta a \to 0} \frac{1}{\Delta a} \int_0^{\Delta a} \overline{\sigma_y}\,\overline{u_y}\, dr \tag{4}$$

where V_m and V_f are volume fraction of the matrix and fibre, respectively, a and d are one-half of the crack size and the fibre diameter, σ_y and u_y are the stress and displacement along the y-axis (see Fig. 2) in the vicinity of the crack tip. σ_y and u_y are given for the homogeneous body with a crack of length $2a$,

$$\sigma_y^i = \sigma_i \left(\frac{a}{2r}\right)^{1/2} \tag{5}$$

$$u_y^i = \frac{4(1-\nu^2)}{(2)^{1/2}E_i} (ra)^{1/2}\, \sigma_i \tag{6}$$

where the super and subscript i denotes m, f for the matrix and fibre phase, respectively. Thus $\overline{\sigma_y}$ and $\overline{u_y}$ are written as

$$\overline{\sigma_y} = \bar{\sigma} \left(\frac{a}{2r}\right)^{1/2} \tag{7}$$

$$\overline{u_y} = \frac{4(1-\nu^2)}{(2)^{1/2}\bar{E}} (ra)^{1/2} \bar{\sigma}. \tag{8}$$

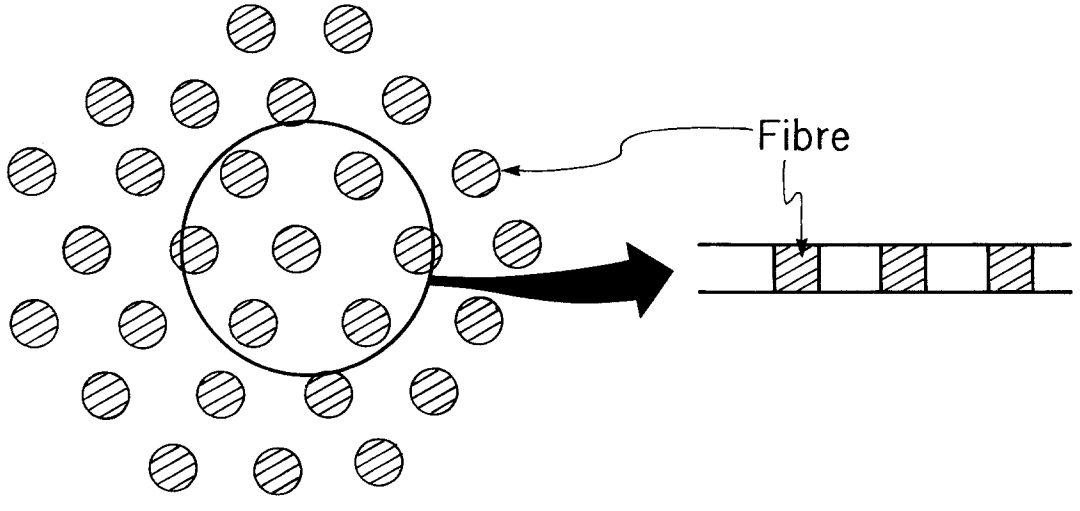

Figure 1 A theoretical model.

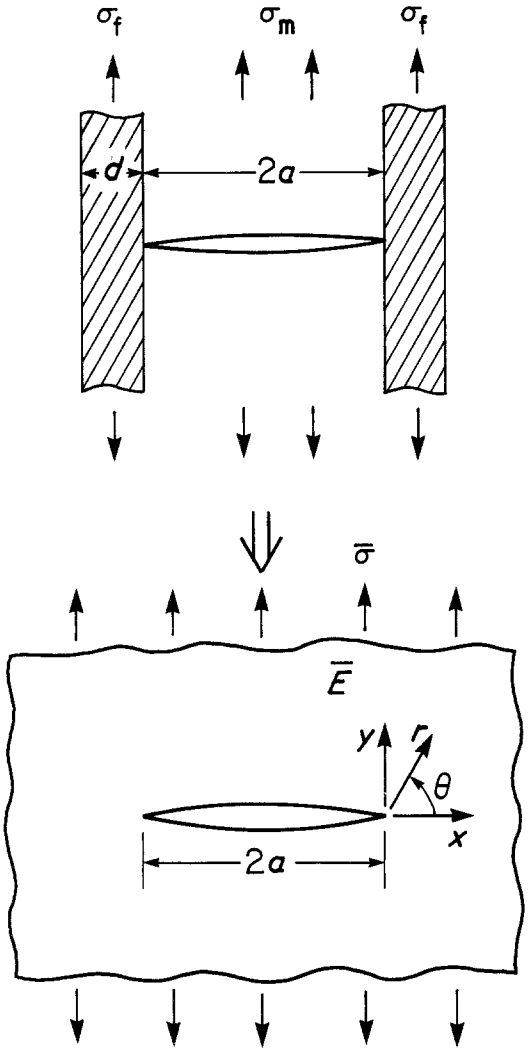

Figure 2 A homogeneous material converted from a composite.

From Equation 5, we obtain

$$\frac{\sigma_y^m u_y^f}{\sigma_y^f u_y^m} = \frac{E_m}{E_f} \tag{9}$$

$$\frac{\sigma_y^m}{\sigma_y^f} = \frac{\sigma_m}{\sigma_f}. \tag{10}$$

By using Equations 2 to 10, we arrive at

$$\bar{G} = \left[V_m \left(\frac{E_m}{\bar{E}} G_m\right)^{1/2} + V_f \left(\frac{E_f}{\bar{E}} G_f\right)^{1/2}\right]^2 \tag{11}$$

where

$$G_i = \frac{\pi(1-\nu^2)\sigma_i^2 a}{E_i}, \qquad i = m \text{ and } f. \tag{12}$$

In the above equations, we have assumed that Poisson's ratio of the two phases are equal:

$$\nu = \nu_m = \nu_f \tag{13}$$

With Equations 3 and 12, Equation 11 is reduced to

$$\bar{G} = \frac{\pi(1-\nu^2)\bar{\sigma}^2 a}{\bar{E}} \tag{14}$$

We note in passing that $\bar{G}$ given by Equation 14 is the energy release rate for a crack of length $2a$, hence $\bar{G}$ can be interpreted as the surface fracture energy for the crack initiation, $2\gamma_I$. In order to compute the contribution of the elastic strain energy to γ_F, we integrate $\bar{G}$ from $a = a_0$ to a_f where a_0 and a_f are the radius of the penny-shaped crack initially and finally when the crack reaches the edge of the specimen, respectively.

2.2. Plastic work along the interface (W_p)

Consider a fibre bridging the crack of size $2a$ as shown in Fig. 3. Under the applied stress, the crack extends and opens, thus resulting in a crack opening displacement (COD) at the point where the fibre intersects the crack. The amount of COD there is denoted by δ_0. The stress in the fibre varies along the fibre axis from a maximum value at the crack plane to the average value at some distance y_0 from the crack plane. Then the work done by the fibre on the matrix above and below the crack plane is given by

$$W_p = 2\pi d \int_0^{y_0} u\,\tau_y\,dy \tag{15}$$

when τ_y is the interfacial shear stress, u is the relative displacement of the fibre to the matrix, and d is the fibre diameter.

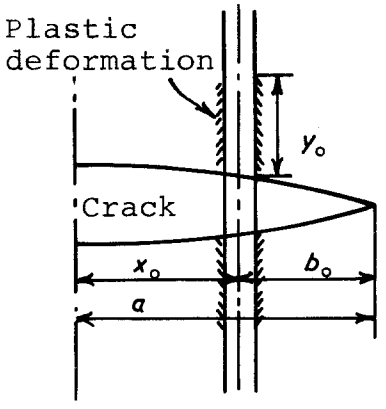

Figure 3 The plastic work in the matrix along the interface.

If τ_y is assumed to be constant and set equal to the matrix shear yield stress, and u is also to be as constant displacement δ_0, then Equation 15 is reduced to

$$W_p = 2\pi d\tau_y \int_0^{y_0} u\,dy$$

$$= 2\pi d\tau_y \delta_0 y_0 \qquad (16)$$

In the above equation, δ_0 is the crack opening displacement at the fibre location and given as the sum of the three cases, (i) the COD, δ_1 by the applied stress, (ii) the COD, δ_2 by the fibre force on the crack plane and (iii) the COD, δ_3 by the frictional force against τ_y over the length y_0 (see Fig. 4). The COD, δ, in general, is related to the stress intensity factor K_I as

$$\delta = \frac{4(1-\nu^2)}{E_m}\left(\frac{b_0}{2\pi}\right)^{1/2} K_I \qquad (17)$$

where

$$K_I = \begin{cases} \bar{\sigma}\,(a\pi)^{1/2} & \text{for } \delta_1 \\ -\dfrac{\sigma_f \pi d^2}{4t(\pi a)^{1/2}}\left(\dfrac{a+x_0}{a-x_0}\right)^{1/2} & \text{for } \delta_2 \\ -\dfrac{\pi d y_0 \tau_y}{t(\pi a)^{1/2}}\left(\dfrac{a+x_0}{a-x_0}\right)^{1/2} & \text{for } \delta_3 \end{cases} \qquad (18)$$

In the above equations $x_0 = a - b_0$ is defined in Fig. 3, t is the thickness of a slice of the composite (Fig. 1) and equal to $\pi d/4$ since we have converted a circular section of the fibre to a rectangular section of d by t. K_I for δ_2 and δ_3 were calculated by Tada *et al.* [13]. y_0 in Equation 16 can be determined from the fracture criterion of the fibre:

$$\frac{\pi d^2 \sigma_{fu}}{4} = \frac{\pi d^2 \sigma_f}{4} + \pi d y_0 \tau_y \qquad (19)$$

where σ_{fu} is the fibre breaking stress. From Equations 16 and 19, the plastic work per unit fibre is obtained as

$$W_p = \pi d^2 (\sigma_{fu} - \sigma_f)\delta_0/2. \qquad (20)$$

2.3. Fibre pull-out energy

Cooper [2] developed a model to calculate the fibre pull-out energy for a continuous composite system where fibres are assumed to have weak points with the average spacing between the weak points, l_w and the strength of the weak, σ^*. By taking account of the mean values of the fibre breaking stress and the fibre pull-out length, Cooper derived the mean value of the fibre pull-out energy per unit fibre, W_{p0} as

$$W_{p0} = \begin{cases} \dfrac{\pi d \tau_y l_w^2}{24} & \text{for } l_w < l_0 \\ \left(\dfrac{\sigma_{fu} - \sigma^*}{\sigma_{fu}} l_c\right)^2 \dfrac{\pi d \tau_y}{24 l_w} & \text{for } l_w > l_0 \end{cases} \qquad (21)$$

where l_0 and l_c are defined by

$$l_0 = \frac{\sigma_{fu} - \sigma^*}{\sigma_{fu}} l_c \qquad (22)$$

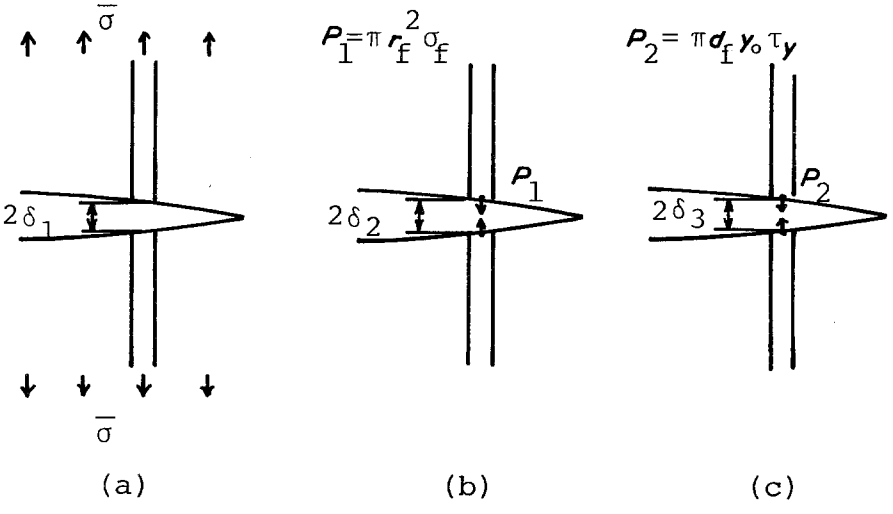

Figure 4 Crack opening displacements by (a) the average stress $\bar{\sigma}$, (b) the average fibre force and (b) the resultant force of the interfacial shear stress.

$$l_c = \frac{d\sigma_{fu}}{4\tau_y} \tag{23}$$

The Cooper's formula requires information which is difficult to obtain, the mean spacing between flaws, l_w and the fibre breaking stress of the weak point σ^*. For simplicity we assume that $l_w = l_c$ and $\sigma^* = \eta\sigma_{fu}$ so that for a given σ^*, we can estimate the maximum value of W_{p0}. Then Equation 21 is reduced to

$$W_{p0} = (1-\eta)^2 \frac{V_f d\sigma_{fu}^2}{64\tau_y} . \tag{24}$$

W_{p0} given by Equation 24 gives the mean value of the fibre pull-out energy per composite. For simplicity the coefficient η in the above equation can be interpreted as the ratio $\sigma_{fu\ lowest}/\sigma_{fu\ mean}$ where $\sigma_{fu\ lowest}$ and $\sigma_{fu\ mean}$ are the lowest and mean values of the fibre breaking stress when a large number of fibres are tested.

2.4. Macroscopic fracture surface energy, γ_F

The total work of fracture, W is the sum of the elastic strain energy release rate and the plastic work, both integrated over the area of the fractured section and W_{p0} defined by Equation 24. Thus, γ_F is given by

$$\gamma_F = \frac{1}{2}\left[\frac{1}{\pi a_f^2}\int_{a_0}^{a_f}\left(2\pi\bar{G} + \frac{8V_f W_p}{d^2}\right) a\,da + \alpha V_f(1-\eta)^2 \frac{d\sigma_{fu}^2}{64\tau_y}\right] \tag{25}$$

where α in the last term of Equation 25 is a fraction of fibres which are pulled-out and have a value from $\alpha = 0$ to $\alpha = 1.0$, and a_0 is the radius of the initial penny-shaped crack and is taken as $b_0/2$ (see Fig. 3), a_f is the effective radius of the fractured section of the specimen.

Substituting Equations 14, 17, 18 and 20 into 25 and performing the integral with respect to a, and then by neglecting the higher order terms, we arrive at

$$\gamma_F = \frac{1}{2}\left[\frac{2\pi^2(1-\nu^2)\bar{\sigma}^2 a_f}{3\bar{E}}(1+\beta) + \alpha V_f(1-\eta)^2 \frac{d\sigma_{fu}^2}{64\tau_y}\right] \tag{26}$$

$$\beta = \frac{8(\sigma_{fu}-\sigma_f)\sigma_{fu}\bar{E}}{\bar{\sigma}^2 E_m} \times \left\{\frac{2}{5}\left(\frac{\bar{\sigma}}{\sigma_{fu}}\right)\left[\frac{1}{2}\left(\frac{b_0}{a_f}\right)\right]^{1/2} - \frac{1}{2\pi}\left(\frac{d}{a_f}\right)\right\}. \tag{27}$$

3. Experiments

In order to verify the analytical formula, Equation 26, we have conducted three-point bending tests for graphite fibre reinforced 6061 aluminium specimens. The geometry and constituents of the composite specimens and experimental apparatus and results compared with the theoretical results are given below.

3.1. Composite specimens

Graphite fibre-reinforced 6061 aluminium sheets are fabricated by Materials Concepts, Inc., Columbus, Ohio. Each sheet has a dimension of 152.4 mm x 152.4 mm x 3.175 mm. Two different volume fractions of fibres are used, 32% and 48%. The

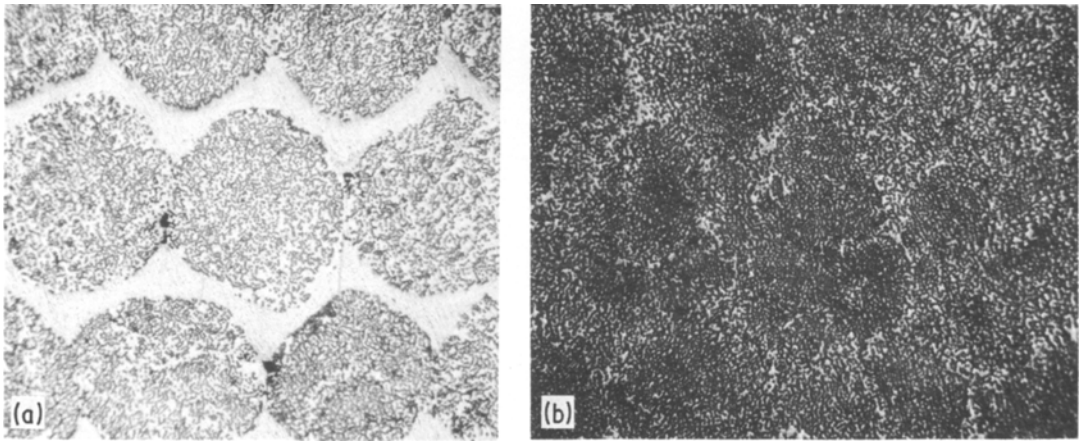

Figure 5 Typical section views by optical microscope with magnification x 33 for (a) $V_f = 32\%$ and (b) $V_f = 48\%$.

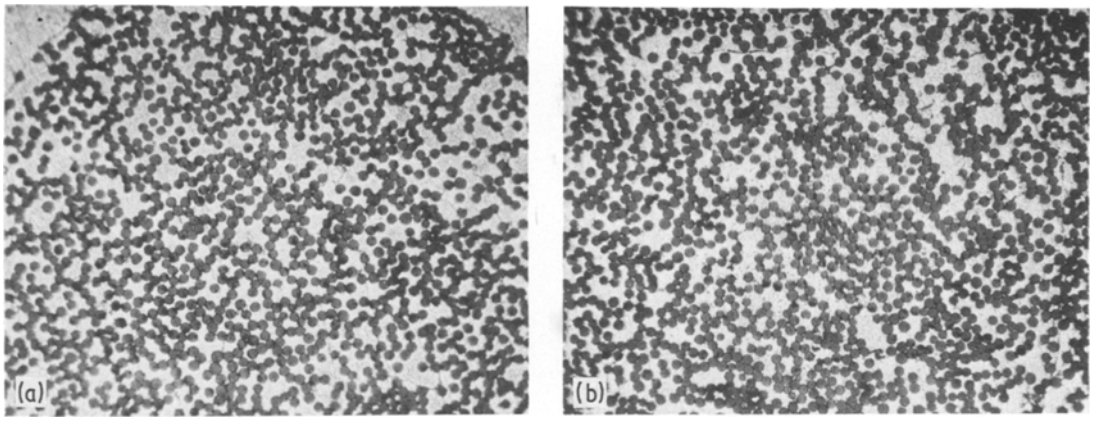

Figure 6 Typical view of graphite fibres in a percursor with magnification × 124 (a) $V_f = 32\%$ and (b) $V_f = 48\%$.

mechanical properties of the fibre and the matrix are:

Fibre: Union Carbide P55
$E_f = 3.78 \times 10^{11}\ \mathrm{N\,m^{-2}}$
$\sigma_{fu} = 2.06 \times 10^{9}\ \mathrm{N\,m^{-2}}$
$d = 1 \times 10^{-5}$ m.

Matrix: Aluminium 6061 – 0 grade
$E_m = 6.47 \times 10^{10}\ \mathrm{N\,m^{-2}}$
$\tau_y = 1.4 \times 10^{8}\ \mathrm{N\,m^{-2}}$
$\nu_m = 0.3$.

Typical sections of 32% and 48% V_f composites are shown in Figs. 5a and b, respectively. It is

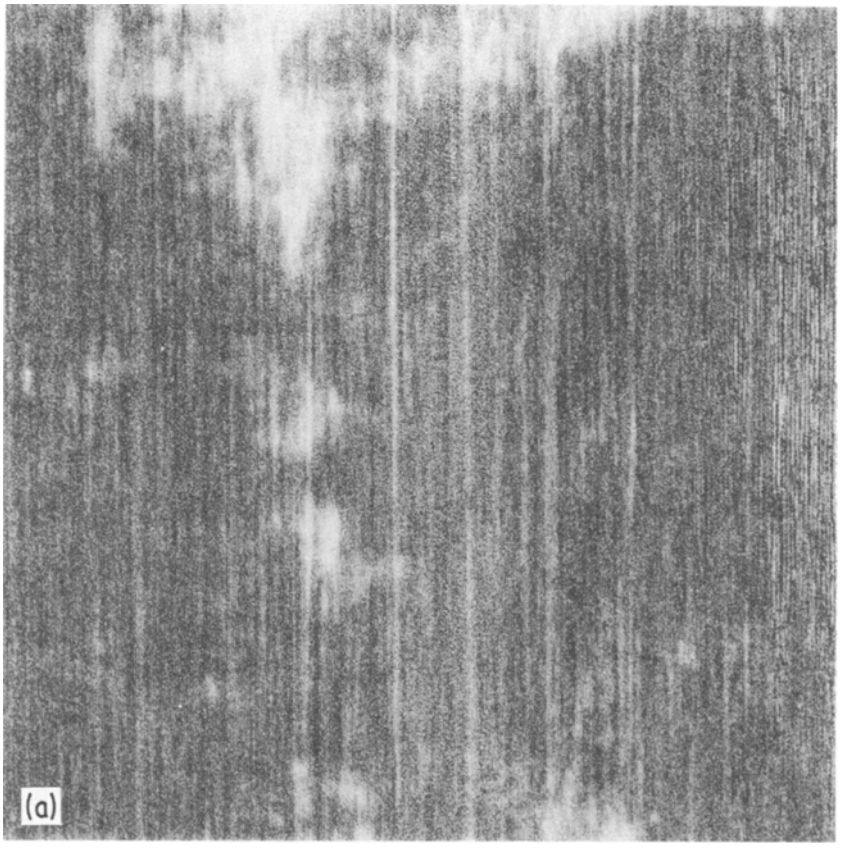

Figure 7 The results of ultrasonic C-scan of the composite sheet for (a) $V_f = 32\%$ and (b) $V_f = 48\%$.

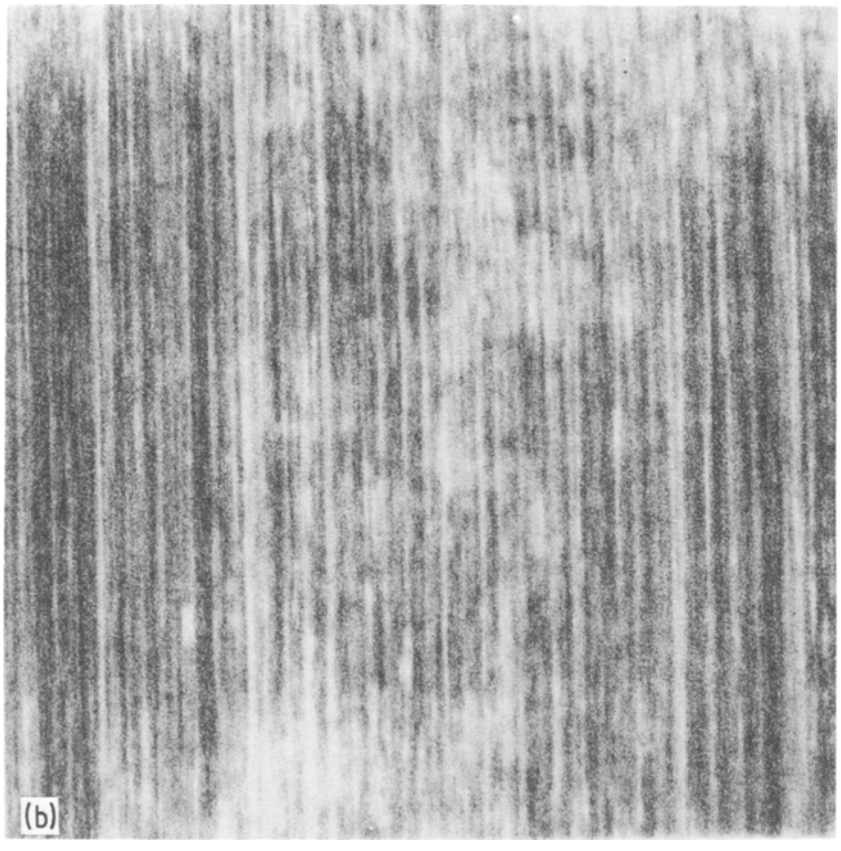

Figure 7 Continued.

seen from Fig. 5 that 32% V_f C–Al composite sheets are made by piling the precursors and 6061 aluminium foils followed by a hot press, and 48% V_f C–Al composite sheets are hot-pressed directly without foils. Each precursor is made by a vacuum infiltration technique. The view of the precursors for 32% V_f and 48% V_f cases at large magnification are shown in Figs. 6a and b, respectively. The pictures of the ultrasonic C-scan of the sheets are shown in Fig. 7 for later convenience. The white spots in Fig. 7 indicate poor bonding which may be caused during the process of hot pressing. The specimen size for the tensile test is 152.4 mm × 10.16 mm × 3.175 mm and that for three-point bending is 71.12 mm × 10.16 mm × 2.54 mm. For the case of the three-point bending test for pure 6061 aluminium, two different specimen sections are used, a square section type (6.35 mm × 6.35 mm) and a flat section type (10.16 mm × 2.54 mm). The specimens for the three-point bending test are notched at their mid span as shown in Fig. 8.

3.2. Experimental results

3.2.1. Tensile test

Tensile tests are conducted on composite specimens with two different volume fractions of fibre, $V_f = 0.32$ and 0.48. The stress–strain curves of the two kinds of composites are shown in Fig. 9. The values of Young's modulus (E) and strength (σ_u) are about 87% and 67% of those calculated by rule of mixture, respectively. Large reduction in E and σ_u is attributed to the fact that the interface between precursors ($V_f = 0.48$) and that between precursor and 6061 aluminium foil ($V_f = 0.32$) was not well bonded as evidenced by the results of ultrasonic C-scan (Fig. 7).

3.2.2. Three-point bending test

A schematic view of a three-point bending test with the geometry of the specimen is shown in Fig. 8 where the load (P)–displacement (δ) curve of the mid-point is also shown. The span between the two end supports is 63.5 mm and the speed of the crosshead of the Instron is set as 0.3 mm min^{-1}.

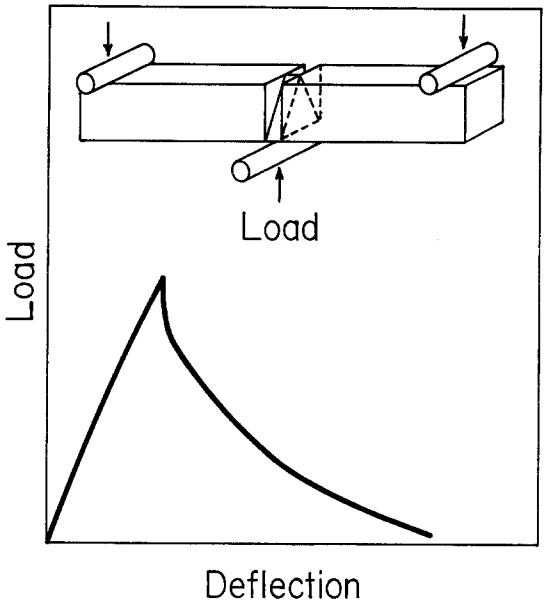

Figure 8 Three-point bending test.

Four different kinds of specimens are used, pure 6061 aluminium with a square section (6.35 mm x 6.35 mm) and with a flat section (10.16 mm x 3.175 mm), 32% V_f C–Al composite and 48% V_f C–Al composite specimens. Both of the C–Al composite specimens have a flat section (10.16 mm x 3.175 mm). The macroscopic fracture surface energy γ_F is computed by $\gamma_F = W/2A$, where W is the total work of fracture and measured by the area underneath the P–δ curve and A is the area of the triangular section at the mid point of the specimen. Six tests are conducted for each type of specimen except for the flat bar 6061 aluminium specimens for which only four tests are performed and the results are listed in Table I. The mean value of γ_F for each case is also given at the right column of the table. It is noted in Table I that we have conducted only four tests for 6061 aluminium specimens of a flat section type (marked by **) and two distinct groups of data were

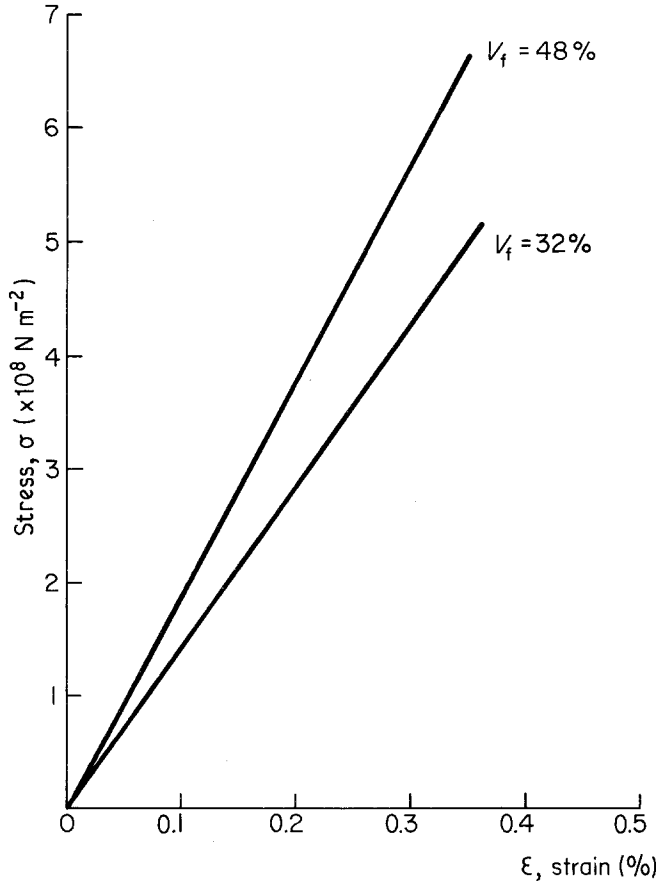

Figure 9 Stress-strain curves of 32% V_f and 48% V_f graphite fibre reinforced 6061 aluminium.

TABLE I γ_F obtained experimentally by three-point bending test

Specimen	Specimen size (mm)	γ_F (kJ m^{-2})	Mean value of γ_F
6061 aluminium	71.12 × 6.35 × 6.35	30.1	
		33.0	
		33.4	35.5
		35.6	
		37.1	
		38.0	
6061 aluminium	71.12 × 10.16 × 2.54	53.0	
		57.9	57.2
		59.0	
		59.0	
		_**	
		_**	
32% V_f C–Al	71.12 × 10.16 × 2.54	5.30	
		5.37	
		5.66	6.05
		6.42	
		6.52	
		7.01	
48% V_f C–Al	71.12 × 10.16 × 2.54	5.15	
		6.03	5.96
		6.28	
		6.37	
		16.5*	17.0
		17.5*	

obtained for 48% V_f C–Al specimens and those with a higher value of γ_F are marked by *, hence the mean value of γ_F was computed for each group.

In order to study the fracture mode of the three-point bending specimens, we have taken the scanning electron microscopy (SEM) pictures for 32% V_f C–Al specimen (Figs. 10a and b) for 48% V_f C–Al specimen with low value of γ_F (Figs. 11a and b) and that with high value of γ_F (Figs. 12a and b). The SEM pictures with the lower magnification (Figs. 10a, 11a and 12a) focus on the fracture mode of the precursors, whereas those with the higher magnification indicate that of each graphite fibre. It follows from these figures that the pull-out of fibres and precursors are more abundant for 48% V_f C–Al specimen of the higher γ_F group than for other C–Al specimens. Thus the pull-out of the fibres and precursors contributes much to the macroscopic fracture surface energy γ_F. This point will be discussed again in detail in the next section.

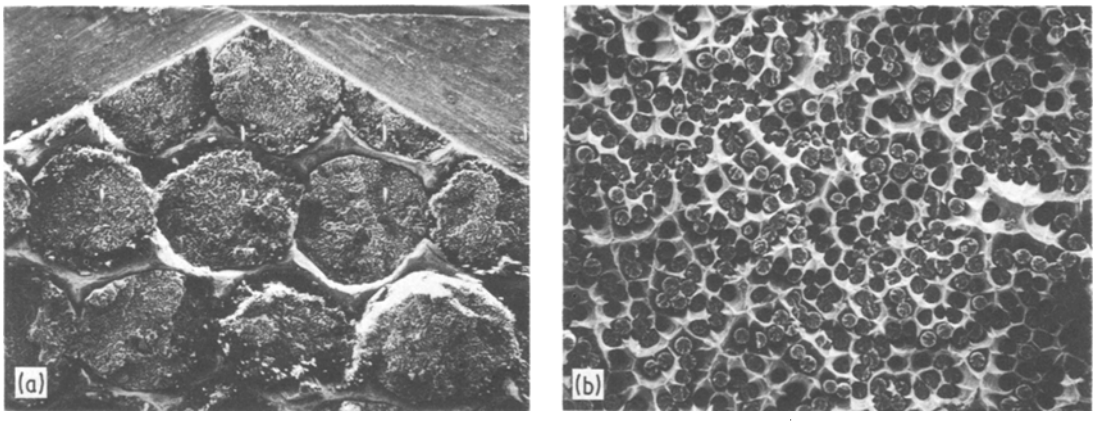

Figure 10 SEM pictures of the fractured section of the three-point bending test of 32% V_f C–Al specimen at the magnification of (a) 25 and (b) 198.

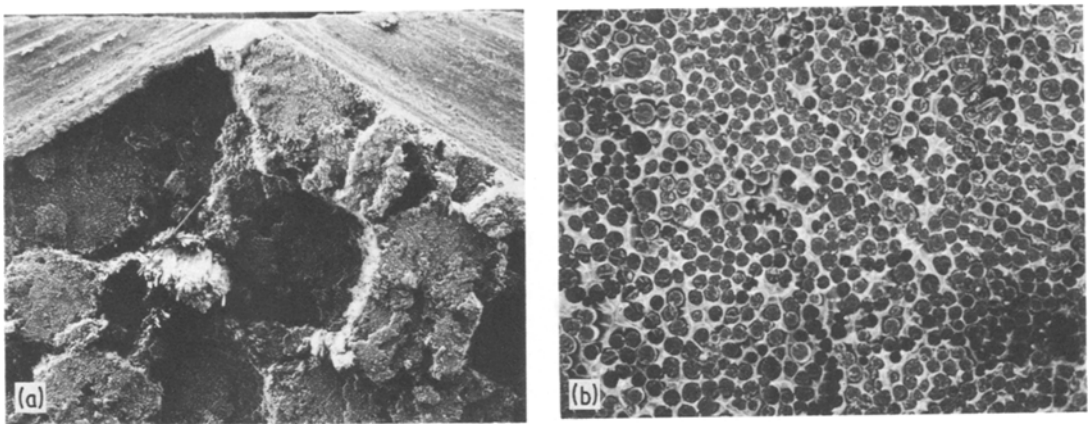

Figure 11 SEM pictures of the fractured section of the three-point bending test of 48% V_f C–Al specimen (first group) at the magnification of (a) 25 and (b) 198.

3.3. Comparison between experimental and theoretical results

First we will obtain the value of γ_F predicted by Equation 26 for the two cases of fibre volume fractions, $V_f = 0.32$ and 0.48. The data common for $V_f = 0.32$ and 0.48 are given below:

$$\nu = 0.3$$

$$E_m = 6.47 \times 10^{10}\ \mathrm{N\,m^{-2}}$$

$$E_f = 3.78 \times 10^{11}\ \mathrm{N\,m^{-2}}$$

$$\sigma_{fu} = 2.06 \times 10^{9}\ \mathrm{N\,m^{-2}}$$

$$d = 1 \times 10^{-5}\ \mathrm{m}$$

$$\tau_y = 1.4 \times 10^{8}\ \mathrm{N\,m^{-2}}$$

$$\sigma_{mu} = 1.26 \times 10^{8}\ \mathrm{N\,m^{-2}}$$

where σ_{fu} and σ_{mu} are the breaking stress of the fibre and matrix, respectively. The data of the matrix is based on 6061 Al–0 grade. The other data for $V_f = 0.32$ and 0.48 are given in Table II. It is noted in Table II that ϵ_0 is defined as the composite failure strain and its value was measured experimentally (Fig. 9).

With the above data, we can compute the value of γ_F predicted by Equation 26. The evaluation of the pull-out energy, the third term in Equation 26, is difficult unless the precise information about the pull-out length of the fibres, the fraction of the fibres being pulled-out and the average spacing of the fibre flaws are known. Thus we first evaluate the first two terms in Equation 26 and then make a rough estimate of the pull-out energy based on the observation of the fractured surface, a fraction α of the fibres and precursors which are pulled-out.

The values of γ_F predicted by the first two terms in Equation 26 are plotted by open triangles

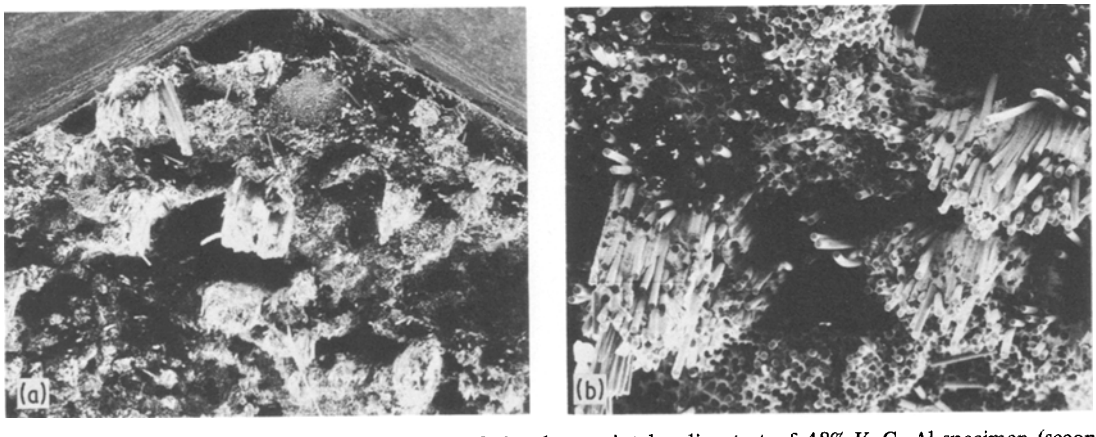

Figure 12 SEM pictures of the fractured section of the three-point bending test of 48% V_f C–Al specimen (second group) at the magnification of (a) 25 and (b) 198.

TABLE II Input data for theoretical evaluation

Parameter	Dimension	$V_f = 0.32$	$V_f = 0.48$
A_f	m	2.111×10^{-3}	2.111×10^{-3}
b_0	m	1.68×10^{-5}	1.37×10^{-5}
$\bar{E}$	$N\,m^{-2}$	1.42×10^{11}	1.89×10^{11}
ϵ_0	1	3.65×10^{-3}	3.55×10^{-3}
σ_m	$N\,m^{-2}$	2.36×10^{8}	2.3×10^{8}
σ_f	$N\,m^{-2}$	1.38×10^{9}	1.34×10^{9}
$\bar{\sigma}$	$N\,m^{-2}$	6.02×10^{8}	7.63×10^{8}

connected by the solid line in Fig. 13. In the same figure the value of γ_F based on the rule of mixtures, $\gamma_F = V_m\gamma_m + V_f\gamma_f$, is shown by a dotted line. The value of γ_m was measured by the three-point bending test and given by Table I where we have chosen γ_m for the specimen of a flat section, i.e. $\gamma_m = 57.2\,kJ\,m^{-2}$. The value of γ_f (graphite) was set as $100\,J\,m^{-2}$ [14]. We have plotted the experimental results (Table I) as open circles with the band of data scattering in Fig. 13. It follows from Fig. 13 that the values of γ_F predicted by the first two terms in Equation 26 agree well with the experimental results except for the case of the second group of 48% V_f C–Al specimens (marked by the asterisk in Table I). The gap between the predicted and experimental results is due to the pull-out of fibres and precursor wires which was not taken into account for the predicted line (the open triangles marks in Fig. 13).

The estimate of the pull-out energy may be far from accurate since the data for several parameters in the third term of Equation 26, α, η and τ_y are not available. Thus the following estimate for the pull-out energy is a very crude approximation. The estimate of a fraction of fibres (or precursors) being pulled-out, α was made by the observation of the SEM fracture pictures (Figs. 10 to 12). The values of η for the fibre and precursor are set as 0.5 and 0.8, respectively, for simplicity. The interfacial shear strength of the precursor may not be the same as that of the fibre, the shear yield stress of 6061 aluminium-0 grade, due to the degradation of the precursors (or the 6061 aluminium foil for the case of 32% V_f C–Al specimens), i.e. the

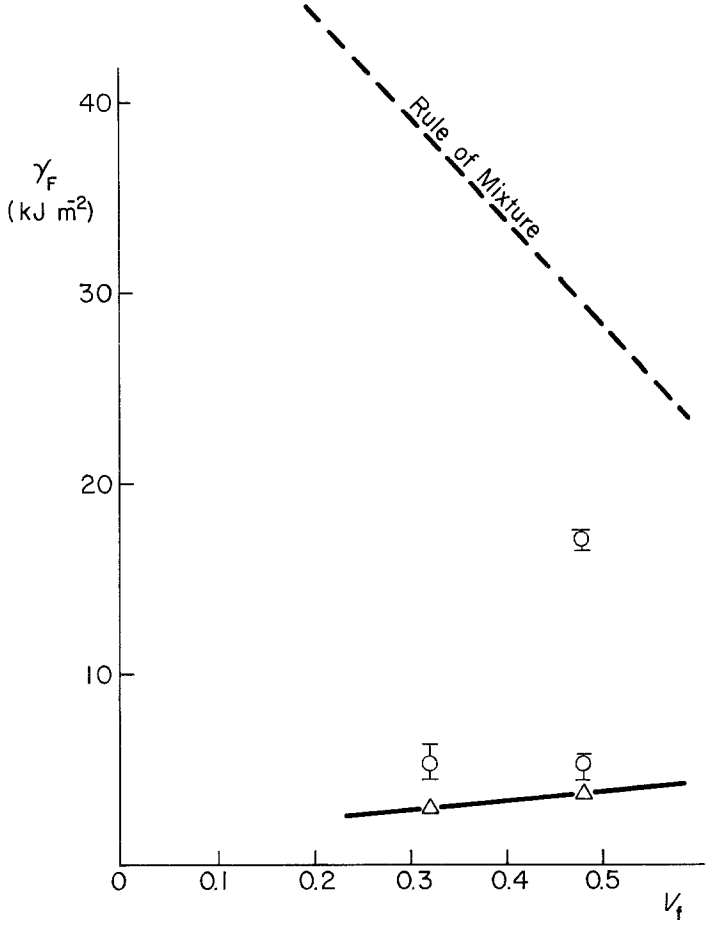

Figure 13 Macroscopic fracture surface energy γ_F as a function V_f. The open circles and triangles denote, respectively, the experimental and theoretical results based on the first two terms in Equation 26.

TABLE III Estimate of pull-out energy

Vf	Fracture section	Fibre pull-out			Wire pull-out			γ_F due to pull-out (kJ m^{-2})
		α	η	Energy (kJ m^{-2})	α	η	Energy (kJ m^{-2})	
0.32	Fig. 10	0.04	0.50	0.04	0.08	0.80	1.7	0.87
0.48	Fig. 11	0.04	0.50	0.06	0.08	0.80	3.7	1.88
0.48	Fig. 12	0.35	0.50	0.50	0.36	0.80	16.7	8.6

oxidation of its surface which we have observed experimentally. However, the value of τ_y for the oxidated surface of 6061 aluminium is not known, hence we have used $\tau_y = 1.0 \times 10^7 \text{N m}^{-2}$ which is lower than the shear yield stress of aluminium. With these crude assumptions, the pull-out energy of the fibre and precursor is calculated using the third term of Equation 26 and the values calculated are tabulated in Table III. When the pull-out energy calculated in the above are added to the values (open triangles), then the total fracture energy γ_F predicted become closer to the experimental results as shown in Fig. 13.

We note again that the values of the pull-out energy estimated here is very crude approximation. For the purpose of a more accurate estimate of the pull-out energy, the data determining, η, τ_y need to be obtained. If the fabrication method for composite sheets is reasonably good, the fracture surface energy γ_F experimentally obtained is close to those predicted as shown in Fig. 13 (32% V_f C–Al and 48% V_f C–Al of the lower value of γ_F).

4. Conclusions

A method of measuring the macroscopic fracture surface energy γ_F was investigated for an unidirectional metal matrix composite system. To this end we have proposed a theoretical model which is compared with the experiment and arrived at the following conclusions:

(i) Three-point bending test for a specimen with a triangular notch at its mid span seems to be a good method to measure γ_F since the measured γ_F agree well with the predicted values.

(ii) It is understood that three-point bending test should be conducted on other types of unidirectional metal matrix composites to obtain more conclusive results.

Acknowledgement

We are thankful for the financial support from Honda Research and Development Company, Japan and discussion with Dr H. Ishikawa, University of Electro-Communications are appreciated.

References

1. M. A. WRIGHT, D. WELCH and J. JOLLAY, *J. Mater. Sci.* 14 (1979) 1218.
2. G. A. COOPER, *ibid.* 5 (1970) 645.
3. M. R. PIGGOTT, *ibid.* 5 (1970) 669.
4. J. K. WELLS and P. W. R. BEAUMONT, *ibid.* 17 (1982) 397.
5. D. C. PHILLIPS and A. S. TETELMAN, *Composites* September (1972) 216.
6. H. ISHIKAWA, T. W. CHOU and M. TAYA, *J. Mater. Sci.* 17 (1982) 832.
7. J. NAKAYAMA, *Amer. Ceram. Soc. J.* 48 (1965) 583.
8. H. G. TATTERSALL and G. TAPPIN, *J. Mater. Sci.* 1 (1966) 296.
9. E. R. THOMPSON, *J. Comp. Mater.* 5 (1971) 235.
10. A. SKINNER, M. J. KOCZAKAND and A. LAWLEY, *Metall. Trans.* 13A (1982) 289.
11. J. E. GORDON and G. JERONIMIDIS, *Roy. Soc. London* A294 (1980) 545.
12. H. ISHIKAWA and M. TAYA, Proceedings of the Fourth International Conference on Composite Materials, Vol. I, Tokyo, November 1982, edited by T. Hayashi *et al.* (Japan Society of Composite Materials) p. 675.
13. H. TADA, P. PARIS and G. IRWIN, "The Stress Analysis of Cracks Handbook" (Del. Res. Corp., 1973).
14. A. KELLY, "Strong Solids", 2nd edn (Oxford, 1973).

Received 7 January
and accepted 24 February 1983